DOI: 10.1002/cjoc.201400690

Interaction of Plasma Proteins with Tri-quaternary Ammonium Salt Cationic Surfactant Studied by QCM-D

Man Xi and Baoyan Zhang*

Research Center for Molecular Science and Engineering, Northeastern University, Shenyang, Liaoning 110819, China

A tri-quaternary ammonium salt cationic surfactant was synthesized. Its structure was confirmed by using Fourier-transform infrared spectroscopy, ^{1}H nuclear magnetic resonance spectroscopy, and X-ray photoelectron spectroscopy analyses. Three model surfaces, including Au-CH_3, Au-OH and Au-COOH, were fabricated. Adsorptions of surfactant on the three model surfaces and subsequent plasma proteins adsorption were investigated by quartz crystal microbalance with dissipation (QCM-D). The mass of surfactant on the Au-COOH surface was the largest, followed by that on the Au-CH_3 surface, and that on the Au-OH surface. These results suggested that the main driving force of surfactant immobilization was electrostatic interaction followed by hydrophobic interaction. Based on the results obtained, we concluded that the protein mass adsorbed on Au-CH_3-**S**, Au-OH-**S**, and Au-COOH-**S** surfaces depended on the protein size and orientation. The mass and thickness of S on the Au-COOH surface is the largest and the protein adsorption capacity of Au-COOH-**S** surface is inferior to that of Au-CH_3-**S**. The Au-COOH-**S** surface could inhibit lysozyme adsorption, maintain the adsorption balance of bovine serum albumin, and induce fibrinogen-binding protein adsorption.

Keywords tri-quaternary ammonium salt cationic surfactant, self-assembled monolayers, quartz crystal microbalance with dissipation (QCM-D), proteins adsorption

Introduction

Tri-quaternary ammonium salt cationic surfactants, as a type of gemini surfactant,[1] have three hydrophilic groups that endow properties superior to those of conventional (monomeric or dimeric) surfactants. These properties include higher surface activity, better solubility, lower critical micelle concentration, more excellent adsorption efficiency, better wetting and so on.[2-4] Quaternary ammonium salt cationic surfactants were first synthesized and studied for their superior performance. Later, they were studied for their bactericidal capabilities.[5] Research on the interaction of tri-quaternary ammonium salts with other materials, such as proteins, is limited, as most studies have focused instead on their synthesis. Tri-quaternary ammonium salts combine the advantages of both polymers and conventional surfactants,[6] thus, they have a great potential for use in various applications.

Proteins are the most abundant and versatile macromolecules in living systems and serve crucial functions in essentially all biological processes; the molecules bind a wide variety of ligands, such as metal ions, bilirubin, fatty acids, drugs, and surfactants.[7-10] Proteins interacting with surfactants are important for fundamental biological systems, protein separation, biosciences, biotechnological processes, drug delivery, cosmetics, and the food industry.[11,12] Ionic surfactants, which are known to show strong associative capacity with proteins in aqueous solutions, present a charged head group attracted to an oppositely charged amino acid residue of a protein and an alkyl chain attracted to nono-polar regions available on the surface and interior of this protein.[13,14]

Several methods for studying the interaction between proteins and surfactants, such as Brewster angle microscopy,[12] small angle neutron scattering,[15] light scattering,[16] and quartz crystal microbalance with dissipation (QCM-D),[17-19] have been developed. Sjöblom *et al*.[20] studied the adsorption of alkyl trimethyl ammonium bromide with alkyl groups onto solid surfaces and measured the adsorption of these surface-active compounds onto model carbon steel compounds directly by QCM-D.

QCM-D is an electromechanical technique that allows simultaneous measurements of changes in frequency related to the coupled mass and energy dissipation related to viscous losses when a molecule in solution binds to the sensor surface.[21] Quartz crystal microbalance (QCM) techniques, in combination with

* E-mail: byzhang2006@126.com; Tel.: 0086-024-83687446; Fax: 0086-024-83687446
Received October 14, 2014; accepted December 2, 2014; published online January 14, 2015.
Supporting information for this article is available on the WWW under http://dx.doi.org/10.1002/cjoc.201400690 or from the author.

the self-assembled monolayers (SAMs) of alkanethiols on gold, constitute powerful tools for investigating the adsorption of surfactants on solid surfaces.[22]

In this paper, a tri-quaternary ammonium salt cationic surfactant (**S**) was prepared, its adsorption on three different alkanethiol SAMs coated on gold chips and subsequent adsorption of three different proteins were investigated by QCM-D.

Experimental

Materials

Bovine serum albumin (BSA) (05470), lysozyme (LYZ) (L6875) and fibrinogen (Fib) (F8630) were obtained from Sigma Chemical Co. 1-Dodecanethiol (98%), 11-mercapto-1-undecanol and 11-mercapto-undecanoic acid (99%) were purchased from Alfa Aesar. Phosphate-buffered saline (PBS 0.9% NaCl, 0.01 mol•L^{-1} phosphate buffer, pH 7.4) used for protein adsorption and surfactant solutions experiment was freshly prepared. Chloroacetyl chloride, *N*,*N*-dimethylpalmitylamine and glycerol were provided by Beijing Chemical Works. All other reagents were analytical reagent grade and used without further purification.

Synthesis of the tri-quaternary ammonium salt cationic surfactant (S) and characterization

The tri-quaternary ammonium salt cationic surfactant (**S**) was synthesized according to previous report.[23] Chloroacetyl chloride (3.20 mol) was added into glycerol (1 mol) under stirring with an absorption instrument of hydrogen chloride. The mixture was heated to 70 ℃ under nitrogen atmosphere and stirred for 3 h. Then excessive chloroacetyl chloride was removed by washing with saturated NaCl aqueous. This solution was extracted with ether. The ether was evaporated by distillation under vacuum at 40 ℃. Intermediate product M_1 was obtained in the yield of 99.6%. M_1 (1.00 mol) reacted with *N*,*N*-dimethylpalmitylamine (2.95 mol) in ethanol for 7 h. The obtained mixture was dried in a vacuum oven for 24 h for ethanol volatilization, then a yellow viscous product was obtained, *i.e.* the tri-quaternary ammonium salt cationic surfactant (**S**) was got with an overall yield of 91%. Its structure is shown in Figure 1.

Fourier transform infrared (FTIR) spectrum of the synthesized surfactant was obtained by the KBr method performed on a PerkinElmer instruments Spectrum One Spectrometer (PerkinElmer, Foster City, CA). ^{1}H nuclear magnetic resonance (^{1}H NMR) (600 MHz) spectrum was obtained using a Bruker-Av 600 spectrometer with $CDCl_3$ as a solvent and tetramethylsilane (TMS) as an internal standard. Atom composition of **S** was analyzed by an ESCA (X-ray photoelectron spectroscopy (XPS), VG Scientific ESCA MK II Thermo Advantage V 3.20 analyzer) equipped with Al Kα at 1486.6 eV and releasing angle of the photoelectron for each atom was fixed at 90°. The sample was completely vacuum dried prior to use. The core-level signals were obtained at a photoelectron take-off angle of 90° with respect to the sample.

Quartz crystal microbalance with dissipation (QCM-D)

The principle of QCM-D is based on the inverse piezoelectric effect of piezoelectric quartz crystal.[24] When the crystal was exposed to a sinusoidal electric field, a shear oscillation could be induced at the resonance frequency and the crystal's oscillation frequency decreased if an increase in mass bound to the quartz surface.[25] For a flat, uniform, and rigid adsorbed layer, Sauerbrey relation can be used to calculate the adsorbed mass.[26]

$$\Delta M = -C\Delta f/n \quad (1)$$

where ΔM represents the adsorbed mass per unit, C is the mass sensitivity constant (17.7 ng•cm^{-2}•Hz^{-1}), and n is the overtone number. However, if the adsorbed layer is not rigid and/or too thick, it will result in a high dissipation shift. In this situation, frequency shift will not be proportional to the change of adsorbed mass. Sauerbrey relation to calculate the adsorbed mass could underestimate the actual mass. Thus, it is necessary to use the Voigt model to calculate the mass and thickness of viscoelastic layer. Voigt model is a common model used to describe the polymer's viscoelasticity property. The model contains a spring and a dashpot as its elements to represent the elastic (storage) and inelastic (damping) behavior of a material, respectively. Using this model in our fitting process, each layer is represented by four unknown parameters: layer density ρ (kg•m^{-3}), layer viscosity η (or G''/ω, kg•ms^{-1}), layer shear modulus μ (or G'', Pa) and layer thickness σ (m). The frequency shift Δf and the dissipation shift ΔD recorded by QCM-D real-time have the relationship with those parameters as follows:[27,28]

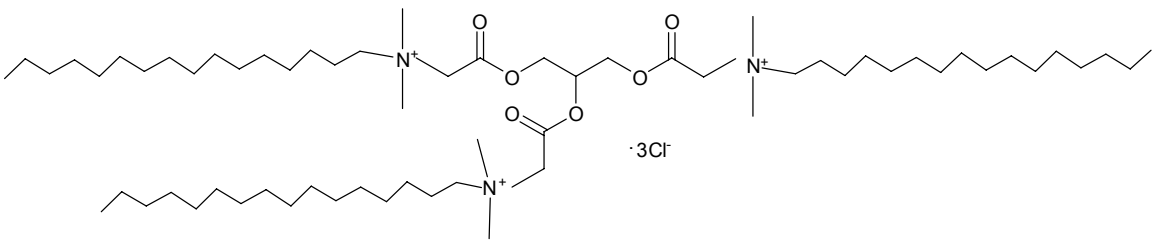

Figure 1 Chemical structure of **S** studied in this work.

$$\Delta f = f_1(n, \eta_f, \rho_f, \mu_f, \sigma_f) \quad (2)$$

$$\Delta D = f_2(n, \eta_f, \rho_f, \mu_f, \sigma_f) \quad (3)$$

$$G^* = G' + jG'' = \mu + j2\pi f\eta \quad (4)$$

In our fitting process, overtones n=3, 5, 7, 9, 11, were used, allowing the model to fit the data and calculate the four unknown parameters (η, ρ, μ, σ) by iterating using QTools software (Q-Sense). Adsorbed layer density was assumed as 1200 kg/m^3 (consider the layer density value between the banding water density 1000 kg/m^3 and protein density 1400 kg/m^3). The density and viscosity of the liquid phase were set as 1000 kg/m^3 and 0.001 kg/ms, respectively. The density of each layer was iterated to find a suitable value then fixed in. The parameters of the layer viscosity, layer shear modulus and layer thickness were set in the range of 0.0001—0.1 kg/ms, 1×10^5—1×10^7 Pa, and 1×10^{-11}—1×10^{-6} m, respectively.

Preparation of tailor-made surfaces and characterization

The AT-cut piezoelecteic quartz crystal disks coated with gold used as QCM-D sensor chips (Q-sense-Biolin Scientific AB, Sweden) had the fundamental frequency of 4.95 MHz and vibrated in the thickness-shear mode with the overtone n of 1, 3, 5, 7, 9, 11, and 13. QCM-D chip was exposed to UV-lamp (185 nm+254 nm) for 15 min to remove organic contaminants, and then was cleaned in a 5∶1∶1 (V∶V∶V) solution of deionized water, ammonia (25%) and hydrogen peroxide (30%) for 5 min at 75 ℃. After excessive rinsing with deionized water, the chip was blown dried with high purity nitrogen for later using.[29]

Self-assembled monolayers (SAMs) of different alkanethiol on gold were used for immobilizing the tri-quaternary ammonium salt cationic surfactant. The cleaned gold chips were immersed in the alkanethiol solutions (1 mmol•L^{-1} 11-mercapto-1-undecanol, 1-dodecanethiol and 11-mercaptoundecanoic acid in ethanol) for at least 16 h in a dark place. They were rinsed with ethanol and then sonicated in ethanol for 5 min twice to remove loosely adsorbed alkanethiols from the surface, and finally dried with high-purity argon shortly before use. Three surfaces, Au-CH_3, Au-OH and Au-COOH were obtained.

Water contact angle measurements were used to study the surface wettability by sessile drop water angle measurement using a contact angle goniometer (DSA 100, KRÜSS GmbH, Hamburg, Germany) by placing 2 μL of distilled water on the surfaces at 25 ℃. For each measurement, clean gold chips presenting different alkanethiol SAM surfaces were put in the holder and introduced into the system. The baseline was corrected according to the position of the gold chip. The contact angle was automatically determined from the base width and height of the individual drops. Six parallel experiments were made on a single sample to obtain the average value of contact angle.

QCM-D procedures

QCM-D procedure was performed to record the immobilization of the tri-quaternary ammonium salt cationic surfactant to tailor-made surfaces and the protein adsorption process (QCM-D E4, Q-sense AB, Gothenburg, Sweden). Surfactant solution (25 mg/mL) in PBS was filtered with Millex-GV 0.22 μm PVDF syringe filters and then degassed by sonication prior to use. A fresh surfactant solution was prepared for each series of measurements. Before our experiment, the instrument channel was cleaned using Hellmanex™ II diluted solution (ϕ=2%, in deionized water) at a flow rate of 30 μL•min^{-1} for 10 h and followed by deionized water at a flow rate of 500 μL•min^{-1} for 2 h to eliminate any contaminant of the instrument.

The immobilization of **S** on different surfaces and the subsequent protein adsorption kinetics were performed on QCM-D. The scheme of surface modification and surfactant immobilization is shown in Figure 2. The QCM-D cell was thoroughly rinsed with PBS buffer between each measurement. After stabilization of the baseline in PBS, surfactant solution was injected for 30 min, and then rinsed off using the PBS solution for 30 min. Thereafter, Fib in PBS was injected with a concentration of 1 mg/mL for 30 min, and then rinsed with buffer. For BSA and LYZ in PBS they were tested with a concentration of 10 mg/mL, and then rinsing with buffer. For all experiments, the flow rate was set to 50 μL/min and temperature was performed at (25±0.05) ℃. Temperature was controlled by the instrument.

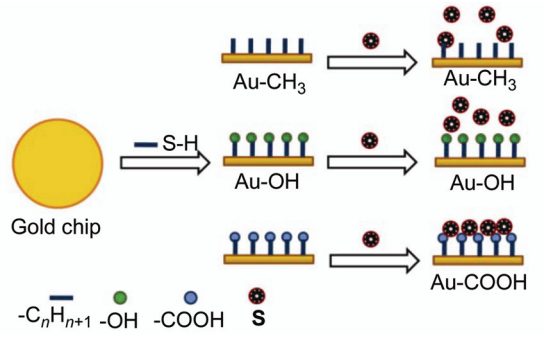

Figure 2 The scheme of surface modification and surfactant immobilization.

Results and Discussion

Characterization of the tri-quaternary ammonium salt cationic surfactant (S)

The chemical structure of **S** was confirmed by FTIR, ^{1}H NMR and XPS analyses (Figure 3). ^{1}H NMR (600 MHz, D_2O) δ: 4.84 (s, 6H), 4.28—4.31 (m, 4H), 3.56 (s, 6H), 3.29 (s, 18H), 1.23—1.27 (m, 78H), 0.82 (t, J=8.0 Hz, 9H); IR (KBr) ν: 3011.60—2960.92, 1765.84—1734.32, 1411.56, 722.27 cm^{-1}.

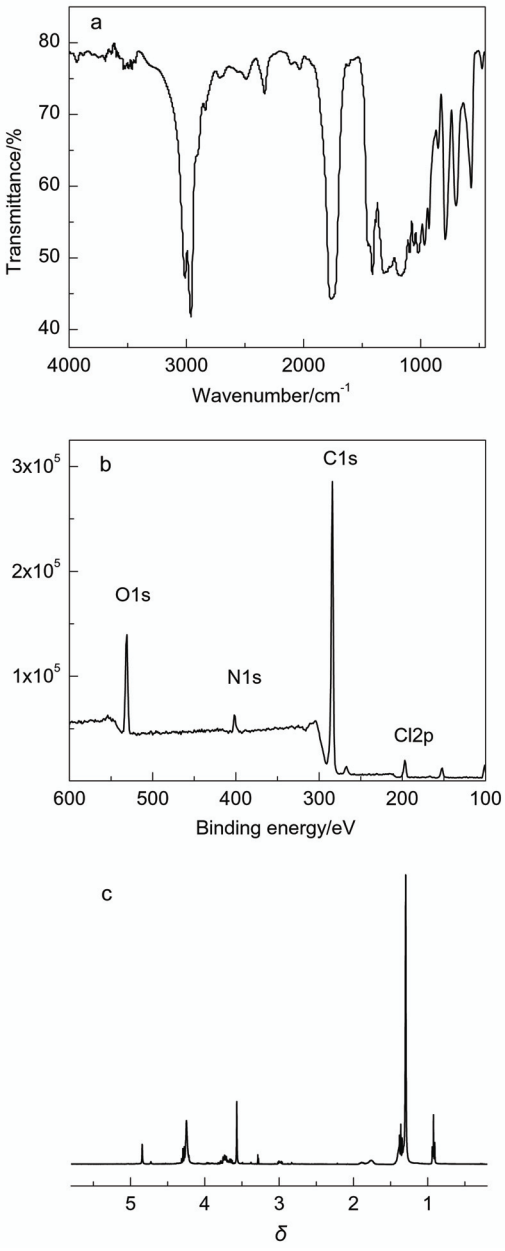

Figure 3 FT-IR (A), XPS (B) and ^{1}H NMR(C) spectra of **S**.

The results above confirm that **S** was fabricated successfully. The XPS spectrum of **S** is used to determine its structure and purity (Figure 3B). Additional N1s (binding energy, 400 eV) and Cl2p (binding energy, 196 eV) peaks in the spectrum of the product prove that the quaternary ammonium salt is formed. The elemental ratio of **S** is determined from XPS as C∶O∶N∶Cl= 20.9∶2.1∶1.3∶1, which is close to the theoretical elemental ratio of 21∶2∶1∶1. The content of N atoms in **S** is higher than that of Cl atoms, which is due to residual *N*,*N*-dimethylhexadecylamine. The purity of **S** is 98.12%. Thus, on the basis of FTIR, ^{1}H NMR, and XPS spectroscopic results, the actual chemical structure of **S** is in good agreement with its predicted structure.

Characterization of tailor-made surfaces

The static water contact angles of different tailor-made surfaces of SAMs are shown in Figure 4. The water contact angle of Au-CH_3 is (97±2)° because of hydrophobicity of the long alkyl chain (1-dodecanethiol). The water contact angles of Au-OH and Au-COOH, which are (42±1)° and (24±2)°, respectively, are attributed to the introduction of polar groups in these surfaces. In addition, the surface of Au-COOH is negatively charged, which can immobilize more cationic surfactant by electrostatic interaction. In this work, we fabricate three tailor-made surfaces with different surface wettabilities and charges.

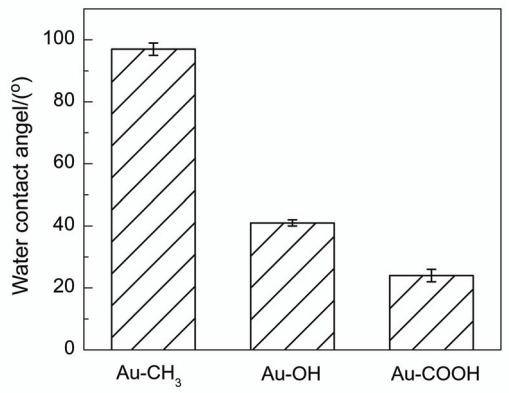

Figure 4 Water contact angles of alkanethiol tailor-made surfaces.

Effect of surface wettability on the immobilized of S

Immobilization of **S** onto the three different surfaces was monitored by QCM-D. Using data of frequencies and dissipation, mass and thickness changes of **S** are simulated by the Voigt model, as shown in Table 1. The values for these outliers are the means of five experiments, so they seem to be statistically verified. The mass and thickness of **S** on the Au-COOH surface is over 20 times those on of the Au-CH_3 surface. Differences between these surfaces can be attributed to electrostatic interactions between the positively charged **S** and negatively charged carboxyl surface. **S** immobilizes on the negatively charged sites of Au-COOH almost exclusively by an ion-exchange mechanism.[30] The interaction between **S** and the Au-CH_3 surface is hydrophobic in nature.

Table 1 Fitting mass and thickness of **S** anti-mobilized on three tailor-made surfaces

Au-CH_3		Au-OH		Au-COOH	
Mass/(ng•cm^{-2})	Thickess/nm	Mass/(ng•cm^{-2})	Thickness/nm	Mass/(ng•cm^{-2})	Thickness/nm
8.9±0.9	89±9.6	0.001	0.01	174.9±1.2	1800±12

The mass and thickness changes of **S** on the surface Au-OH are approximately zero, which means the surfactant is hardly immobilized on the hydrophilic hydroxyl surface. The hydroxyl groups are so much more efficient than carboxyl and alkyl groups at preventing cationic surfactant adsorption. Thus, the main driving force of immobilizing cationic three-chain surfactant is electrostatic interaction, followed by hydrophobic interaction.

In addition, we investigate the relation of frequency and dissipation changes of **S** on the surfaces of Au-CH_3 and Au-OH to explain the dynamic immobilization process. In general, an increase in $-\Delta f$ indicates an increase in the coupled mass to the quartz crystal, whereas an increase in ΔD indicates increased viscous loss and thickness to the adsorbed layers. In Figure 5, the relation of frequency and dissipation of **S** on the Au-CH_3 surface shows an initial monotone increase and then a subsequent monotone decrease up to a frequency of −8 Hz. This observation indicates that the immobilization of **S** on the hydrophobic surface is a completing process, which is combined with anchoring surfactant onto surface and hydration of surfactant with water. Finally, anchoring surfactant is favored because of hydrophobic interaction. By contrast, on the Au-OH surface, the relation of frequency and dissipation shows an initial monotone increase and then a monotone decrease to negative values. This result suggests that hydration between surfactant in water takes a leading role in the immobilization. Therefore, the amount of **S** adsorbed on the surface of Au-COOH is the largest, followed by that on Au-CH_3, and then that on Au-OH, which shows hardly any surfactant (Figure 2).

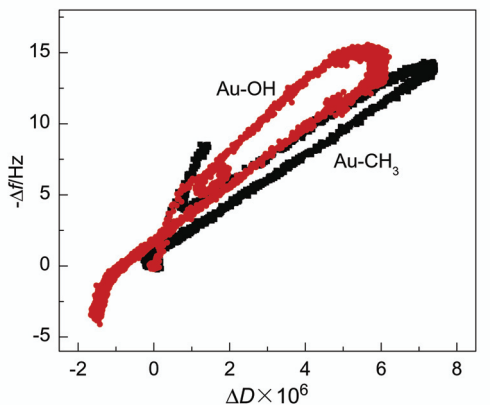

Figure 5 The relation of frequency and dissipation of **S** immobilized on the Au-CH_3 and Au-OH surfaces.

Interactions of plasma proteins with S

In this study, bovine serum albumin (BSA, 14.0 nm×4.0 nm×4.0 nm), fibrinogen (Fib, 47 nm×5 nm ×5 nm),[31] and lysozyme (LYZ, 4.5 nm×3.0 nm×3.0 nm) were used as model proteins to investigate the interaction between proteins and **S**.[32-34] BSA is a small and highly abundant plasma protein that maintains colloidal osmotic pressure and transports some small molecules in the blood.[35] Fib is a rodlike protein that plays a vital role in coagulation, platelet activation, and aggregation.[36] LYZ is a small globular protein consisting of 129 amino acids and usually used as a preserving agent for cheese and tinned vegetables.[37] It is generally recognized that the adsorption of protein at solid interfaces is controlled mainly by the properties of charge and hydrophobicity of the surface. The frequency changes (Δf) and dissipation changes (ΔD) of proteins are given in Figure 6 and Table 2, respectively.

Figure 6 shows that the frequencies of LYZ on the immobilized surfactant surfaces are lower than that on unmodified surfactant surfaces, especially for the Au-CH_3 surface. On the surface of hydrophobic Au-CH_3, the frequency change of LYZ adsorption is about −15 Hz, while the frequency change of LYZ adsorption on the surface of Au-CH_3-**S** is nearly zero. ΔD of Au-CH_3 and Au-CH_3-**S** surfaces are almost zero, suggesting the formations of rigid LYZ layers on the two surfaces.[37] These changes indicate that **S** immobilized on the Au-CH_3 surface can efficiently decrease the adsorption of positively charged LYZ because of electrostatic repulsion. This repulsion is the most obvious on the hydrophobic surface.

On the Au-COOH surface, the frequency change of LYZ adsorption is about −20 Hz, while the frequency change of LYZ adsorption on the Au-COOH-**S** surface is only −8 Hz. ΔD of Au-COOH surface is zero, because LYZ molecules are very small which can combine with the COOH surface and then stay among chains. While ΔD of Au-COOH-**S** surface is 0.4×10^{-6}, the cause of D increase is the electrostatic repulsion of **S** with LYZ. Thus, the Au-COOH-**S** surface can inhibit the adsorption of LYZ and we can conclude that **S** can decrease interaction between LYZ and a surface and inhibit adsorption, thereby providing a theoretical basis for research on protein separation.

The mechanisms of adsorption of negatively charged proteins (*e.g.*, BSA and Fib) on the surfaces are complicated. Frequency changes of BSA and Fib on the surfaces of Au-OH-**S** and Au-CH_3-**S** have lower values, compared with the surfaces of Au-OH and Au-CH_3. This result means more BSA and Fib molecules are adsorbed on the surfaces of Au-OH-**S** and Au-CH_3-**S** then on the surfaces of Au-OH and Au-CH_3 because of the electrostatic interaction between the **S** surface and negatively charged proteins. Introduction of **S** does not significantly affect the adsorption of small-sized BSA on the Au-COOH-**S** surface but greatly affects the adsorption of Fib. The frequency changes of large sized Fib on the surfaces of Au-COOH and Au-COOH-**S** are −57 Hz (Figure 6C) and −81 Hz (Figure 6F), respectively. And corresponding notable increase in ΔD relative to the baseline further indicates the adsorption of fibrinogen which may form a viscoelastic layer on the two surfaces. So the surfactant can induce Fib to adsorb on the Au-COOH-**S** surface.

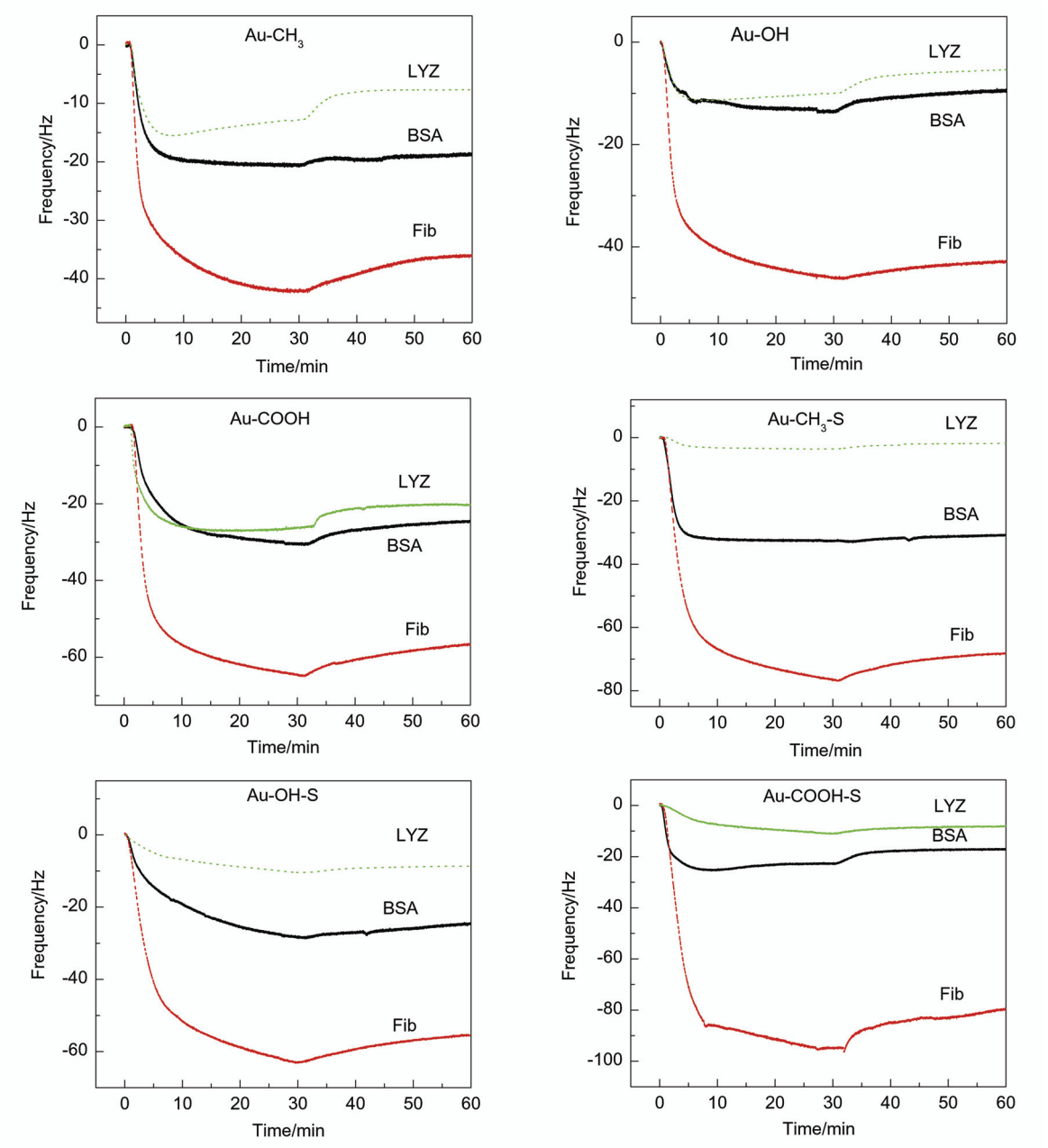

Figure 6 Frequency changes of proteins injected on different surfaces.

Table 2 Dissipation changes of proteins injected on different surfaces.

	$Au\text{-}CH_3$	$Au\text{-}CH_3$-**S**	Au-OH	Au-OH-**S**	Au-COOH	Au-COOH-**S**
Fib	3.6×10^{-6}	3.9×10^{-6}	2.3×10^{-6}	2.8×10^{-6}	2.5×10^{-6}	3.7×10^{-6}
BSA	0.5×10^{-6}	1.1×10^{-6}	0	0.4×10^{-6}	3.0×10^{-6}	1.3×10^{-6}
LYZ	0.4×10^{-6}	0.1×10^{-6}	0.5×10^{-6}	1.2×10^{-6}	0	0.4×10^{-6}

The frequency changes of BSA basically have no difference on the surfaces of Au-COOH and Au-COOH-**S**. Despite BSA has hydrophilicity and negative charge, its adsorption on the Au-COOH surface is attributed to the charge heterogeneity of BSA: positively charged amine groups were present even though the net charge was negative.[38] There are many positive charges in Au-COOH-**S** surface, the strong electrostatic interaction between BSA and **S** results in BSA adsorbed on the Au-COOH-**S** surface. The results demonstrate the balance between the BSA and **S** attraction and the amine groups in BSA and carboxylic group interaction on the Au-COOH surface. Taken together, protein screening and separation may be achieved through regulation of the interactions between surfactant and relevant interfaces.

CHINESE JOURNAL OF CHEMISTRY

Figure 7 shows the adsorbed mass and thickness of the three proteins on the Au-CH_3-**S**, Au-OH-**S**, and Au-COOH-**S** surfaces. The changed trend of protein mass on the three surfaces differs with protein sizes and orientations. The adsorbed masses of BSA and Fib on the Au-CH_3-**S** surface are 559.7±2.9 and 2568.3±13.9 ng/cm^2, respectively; the two proteins represent the largest adsorbed masses among the three surfaces. The theoretical adsorption amounts of BSA on a surface with end-on and side-on close-packed monolayer coverage are 720 and 210 ng/cm^2, respectively.[39] BSA adsorbed on the Au-CH_3-**S**, Au-OH-**S** and Au-COOH-**S** surfaces presents a mixture of side-on and end-on orientations. The theoretical adsorption amounts of Fib on a surface with side-on and end-on close-packed monolayer coverage are 240 ng/cm^2 and 2260 ng/cm^2, respectively.[40] These values suggest that the Fib adsorbed on the surface of Au-CH_3-**S** presents an end-on orientation. Although the mass and thickness of **S** on the Au-COOH surface is over 20 times those on the Au-CH_3 surface (Table 1), the protein adsorption capacity of Au-COOH-**S** is inferior to that of Au-CH_3-**S**. On the surface of Au-CH_3-**S**, the positive charge of **S** is preserved to the utmost extent, which provides more sites for combining with negatively charged protein. However, on the Au-COOH surface, the positive charge of **S** is neutralized by carboxylic groups. Thus, the adsorbed mass on this surface is lower than that on Au-CH_3 surface. In addition, the adsorbed masses of LYZ on the three surfaces show an inverse relationship with the amount of surfactant. LYZ can replace the surfactant immobilized on the Au-COOH-**S** surface, because the protein features an excess of eight positive charges, which can compete with the **S** to combine with carboxylic groups. This leads to the mass and thickness of LYZ on the Au-COOH-**S** surface reducing even to be negative (Figure 7).

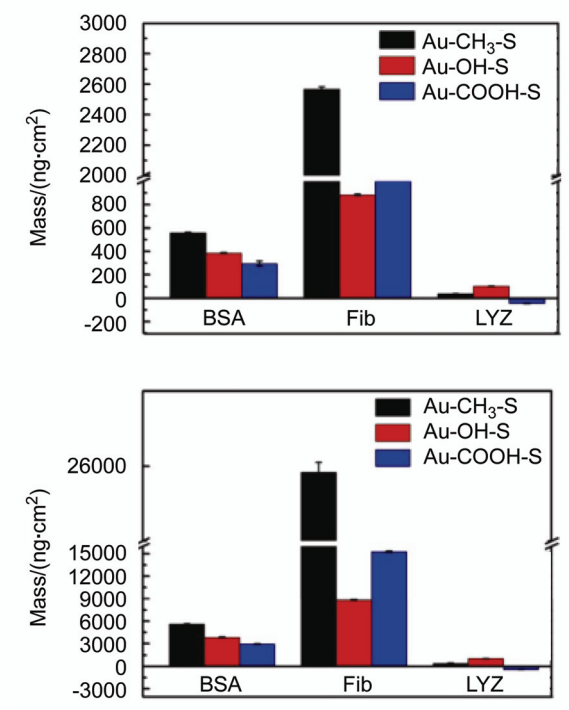

Figure 7 The mass and thickness changes of plasma proteins on different surfaces.

Therefore, a scheme representing the adsorption of the three proteins on the Au-COOH and Au-COOH-**S** surfaces is provided in Figure 8. Figure 8A shows that the Au-COOH surface can adsorb a number of LYZ molecules due to electrostatic interaction, whereas the Au-COOH-**S** surface can inhibit the adsorption of LYZ, and **S** on the surface can be replaced by the approaching LYZ molecules. In Figure 8B, no obvious difference in BSA adsorption is observed on the surfaces of Au-COOH and Au-COOH-**S**. The BSA adsorbed on the Au-COOH-**S** surface presents a mixture of side-on and end-on orientations. This finding can be attributed to the balance between the BSA and **S** attraction and the amine groups in BSA and carboxylic group interaction on the Au-COOH surface. The Au-COOH-**S** surface induces Fib adsorption, as shown in Figure 8C, which is the result of electrostatic attraction between **S** and Fib.

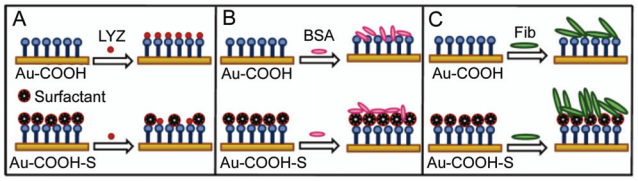

Figure 8 Schematic representing proteins adsorption on Au-COOH and Au-COOH-**S** surfaces.

Conclusions

In this study, a tri-quaternary ammonium salt cationic surfactant (**S**) was fabricated, and its structure and composition were confirmed by FTIR, ^{1}H NMR, and XPS analysis. The adsorption of **S** on three model surfaces and subsequent plasma proteins adsorption were investigated by QCM-D. The mass of surfactant on the Au-COOH surface is the largest, followed by that on the Au-CH_3 surface, and that on the Au-OH surface. These observations suggest that the main driving force of **S** immobilization is electrostatic interaction followed by hydrophobic interaction. The protein mass adsorbed on Au-CH_3-**S**, Au-OH-**S**, and Au-COOH-**S** depended on the protein size and orientation. BSA adsorbed on the Au-CH_3-**S**, Au-OH-**S**, and Au-COOH-**S** surfaces present a mixture of side-on and end-on orientations. The Fib adsorbed on the surface of Au-CH_3-**S** presents an end-on orientation. The adsorbed masses of LYZ on the three surfaces show an inverse relationship with the amount of surfactant. While the mass and thickness of **S** on the Au-COOH surface is over 20 times larger than those on Au-CH_3 surface, the protein adsorption capacity of Au-COOH-**S** is inferior to that of Au-CH_3-**S**; this result can be attributed to preservation of positive charges on the Au-CH_3-**S** surface. The Au-COOH-**S**

surface inhibited LYZ adsorption, maintained the adsorption balance of BSA, and induced Fib adsorption. These results can be used for protein screening and separation applications.

Acknowledgement

The authors thank the National Natural Science Fundamental Committee of China and HI-Tech Research and the Development Program (863, No. 2006AA02Z291) of China.

References

[1] Kim, T. S.; Kida, T.; Nakatsuji, Y.; Ikeda, I. *Langmuir* **1996**, *12*, 6304.
[2] Bakshi, M. S.; Singh, K. *J. Colloid Interface Sci*. **2005**, *287*, 288.
[3] Zheng, O.; Zhao, J. *J. Colloid Interface Sci*. **2006**, *300*, 749.
[4] Bell, P. C.; Bergsma, M.; Dolbnya, I. P.; Bras, W.; Stuart, M. C. A.; Rowan, A. E.; Feiters, M. C.; Engberts, J. B. F. N. *J. Am. Chem. Soc*. **2003**, *125*, 1551.
[5] Parreira, H. C.; Lukenbach, E. R.; Lindeman, M. K. O. *J. Am. Oil Chem. Soc*. **1979**, *56*, 1015.
[6] Zerpa, L. E.; Queipo, N. V.; Pintos, S.; Salager, J. L. *J. Pet. Sci. Eng.* **2005**, *47*, 197.
[7] De, S.; Girigoswami, A.; Das, S. *J. Colloid Interface Sci*. **2005**, *285*, 562.
[8] Vasilescu, M.; Angelescu, D.; Almgren, M.; Valstar, A. *Langmuir* **1999**, *15*, 2635.
[9] Watanabe, S.; Sato, T. *BBA-Gen. Subjects* **1996**, *1289*, 385.
[10] Sulkowska, A. *J. Mol. Struct*. **2002**, *614*, 227.
[11] Douliez, J. P.; Sy, D.; Vovelle, F.; Marion, D. *Langmuir* **2002**, *18*, 7309.
[12] Mackie, A. R.; Gunning, A. P.; Ridout, M. J.; Wilde, P. J.; Patino, J. R. *Biomacromolecules* **2001**, *2*, 1001.
[13] Guo, X.; Yan, H.; Guo, R. *Chin. J. Chem*. **2008**, *26*, 1589.
[14] Jia, L.; Xu, L.; Wang, Z.; Xu, J.; Ji, J. *Chin. J. Chem*. **2014**, *32*, 85.
[15] Stenstam, A.; Montalvo, G.; Grillo, I.; Gradzielski, M. *J. Phys. Chem. B* **2003**, *107*, 12331.
[16] Valstar, A.; Almgren, M.; Brown, W.; Vasilescu, M. *Langmuir* **2000**, *16*, 922.
[17] Tehrani-Bagha, A. R.; Holmberg, K. *Langmuir* **2008**, *24*, 6140.
[18] Naderi, A.; Claesson, P. M. *Langmuir* **2006**, *22*, 7639.
[19] Boschkova, K.; Feiler, A.; Kronberg, B.; Stalgren, J. J. R. *Langmuir* **2002**, *18*, 7930.
[20] Knag, M.; Sjöblom, J.; Øye, G.; Gulbrandsen, E. *Colloid Surface A* **2004**, *250*, 269.
[21] Rodahl, M.; Hook, F.; Fredriksson, C.; Keller, C. A.; Krozer, A.; Brzezinski, P.; Voinova, M.; Kasemo, B. *Faraday Discuss*. **1997**, *107*, 229.
[22] Oskarsson, H.; Frankenberg, M.; Annerling, A.; Holmberg, K. *J. Surfactants Deterg*. **2007**, *10*, 41.
[23] Xie, Y. J.; Yan, F.; Chen, M. S.; Ge, J. J.; Wang, M. X.; Li, J. X.; Zhu, S. *Fine Chem*. **2011**, *28*, 659 (in Chinese).
[24] Hu, Y.; Jin, J.; Han, Y.; Yin, J.; Jiang, W.; Liang, H. *RSC Adv*. **2014**, *4*, 7716.
[25] Hemmersam, A. G.; Foss, M.; Chevallier, J.; Besenbacher, F. *Colloid Surface B* **2005**, *43*, 208.
[26] Palmqvist, L.; Holmberg, K. *Langmuir* **2008**, *24*, 9989.
[27] Domack, A.; Prucker, O.; Rühe, J.; Johannsmann, D. *Phys. Rev. E* **1997**, *56*, 680.
[28] Voinova, M. V.; Rodahl, M.; Jonson, M.; Kasemo, B. *Phys. Scripta* **1999**, *59*, 391.
[29] Kern, W. *RCA Rev*. **1970**, *31*, 187.
[30] Xu, S.; Boyd, S. A. *Environ. Sci. Technol*. **1995**, *29*, 312.
[31] Sigal, G. B.; Mrksich, M.; Whitesides, G. M. *J. Am. Chem. Soc*. **1998**, *120*, 3464.
[32] Gelamo, E.; Silva, C.; Imasato, H.; Tabak, M. *BBA-Protein Struct. Mol. Enzym*. **2002**, *1594*, 84.
[33] Malcolm, A. S.; Dexter, A. F.; Middelberg, A. P. *Langmuir* **2006**, *22*, 8897.
[34] Morén, A. K.; Khan, A. *Langmuir* **1998**, *14*, 6818.
[35] Zhang, C.; Jin, J.; Zhao, J.; Jiang, W.; Yin, J. *Colloid Surface B* **2013**, *102*, 45.
[36] Jin, J.; Jiang, W.; Zhao, J.; Yin, J.; Stagnaro, P. *Appl. Surf. Sci*. **2012**, *258*, 5841.
[37] Jollès, P. *Lysozymes*: *Model Enzymes Biochemistry and Biology*, Springer, New York, **1996**.
[38] Contreras, A. E.; Steiner, Z.; Miao, J.; Kasher, R.; Li, Q. *Environ. Sci. Technol*. **2011**, *45*, 6309.
[39] Wertz, C. F.; Santore, M. M. *Langmuir* **1999**, *15*, 8884.
[40] Wertz, C. F.; Santore, M. M. *Langmuir* **2001**, *17*, 3006.

(Zhao, C.)

